Catal Lett (2009) 128:475–482
DOI 10.1007/s10562-008-9775-z

The Effect of Al_2O_3 Doping into TiO_2–ZrO_2 on the Storage and Sulfur-resistance Performance of the NO_x Trap Catalyst Pt/K/TiO_2–ZrO_2

Zhi-Qiang Zou · Ming Meng · Xiao-Yan Zhou · Xin-Gang Li · Yu-Qing Zha

Received: 6 October 2008 / Accepted: 9 November 2008 / Published online: 21 November 2008

Abstract A series of lean-burn NO_x trap (LNT) catalyst Pt/K/Al_2O_3–TiO_2–ZrO_2 were prepared by sequential impregnation with the support synthesized by coprecipitation. The effect of Al_2O_3 doping into TiO_2–ZrO_2 on the storage and sulfur-resistance performance of the catalyst Pt/K/TiO_2–ZrO_2 was investigated carefully. In situ DRIFTS spectra show that the NO_x is mainly stored as nitrate at the optimal temperature of ~350 °C. The NO_x storage capacity (NSC) of Pt/K/TiO_2–ZrO_2 was greatly improved by Al_2O_3 doping due to the remarkably increased specific surface area and the decreased Ti content. The results of sulfation and regeneration by H_2-TPR reveal that the sulfur on Al_2O_3–TiO_2–ZrO_2 supported catalysts is easier to be removed, making them possess much better sulfur-resisting ability than TiO_2–ZrO_2 or Al_2O_3 supported ones. The NSC recovery efficiency of Al_2O_3–TiO_2–ZrO_2 supported catalysts can reach as high as 81–96% while only 30.4 and 62.5% were achieved for the catalysts supported on pure Al_2O_3 and TiO_2–ZrO_2, respectively. The doped catalyst with the Al/(Ti + Zr) atomic ratio of 3:1 always shows the highest NSC before or after sulfation-regeneration.

Keywords Al_2O_3–TiO_2–ZrO_2 · NO_x storage · Sulfur-resistance · Potassium

1 Introduction

Lean-burn NO_x trap (LNT) catalyst system is a great solution to increasing fuel economy, decreasing emission of carbon dioxide and hydrocarbons, and removing poisonous NO_x which can not be effectively reduced to N_2 over traditional three-way catalysts under lean burn condition. The first generation of LNT catalyst was proposed by Toyota in the middle of 1990s [1, 2]. It mainly consists of three major components: (1) noble metals, such as Pt or Pt-Rh for NO_x oxidation and reduction; (2) alkali or alkaline oxides, such as BaO, used for NO_x storage; (3) Al_2O_3 support with a large specific surface area for providing a high dispersion of the other components. The storage and reduction process can be described as follows: during lean-burn condition, the NO_x is oxidized and stored as nitrates in the storage component; when the engine is switched to a reducing atmosphere, the NO_x stored as nitrates is released and reduced to N_2 by carbon monoxide and hydrocarbons.

Although the LNT catalyst has been put into market in Japan where the fuel is nearly free of sulfur, it cannot be extensively applied in many other countries due to the relatively high content of sulfur in the fuel, which readily leads to deactivation of LNT catalyst. SO_2 and NO_x, both as acidic gases, are competitive for the same adsorption sites, and sulfate is easier to form than nitrate because of its higher thermodynamic stability. During lean-burn period, sulfur oxides can poison both the basic storage component and the support [3–7]. In addition, under rich-burn condition, sulfur can also accumulate on the noble metal component, and consequently decrease its oxidation ability [8, 9]. The addition of the transition metal to the LNT catalysts seems to be a way to improve the sulfur tolerance. By comparing the additive components such as Fe, Co, Ni, and Cu, Yamazaki et al. [10] found that Fe could effectively promote sulfate decomposition by suppressing the growth of sulfate particles. However, Luo et al. [11] found that the introduction of Fe to the Pt/Ba/Al_2O_3 catalyst decreases the Pt–Ba interaction by encapsulation of Pt in

Z.-Q. Zou · M. Meng (✉) · X.-Y. Zhou · X.-G. Li · Y.-Q. Zha
Tianjin Key Laboratory of Applied Catalysis Science & Engineering, Department of Catalysis Science & Technology, School of Chemical Engineering & Technology, Tianjin University, 300072 Tianjin, People's Republic of China
e-mail: mengm@tju.edu.cn

the matrix of Fe/FeOx lattice after repeated redox cycles, leading to the decrease of NO_x storage capacity (NSC) of the catalyst, and making sulfur removal more difficult, since Fe selectively catalyzes the reduction of $BaSO_4$ into BaS.

Recently, a new LNT catalyst Pt/K/TiO_2–ZrO_2 defined as the third generation of LNT catalyst previously [12, 13] has been put forward, using acidic binary oxides as a support. The acidity of this kind of support can prevent SO_2 adsorption and promote SO_2 desorption, largely increasing the sulfur-resisting ability of the LNT catalyst, as compared with the traditional Pt/Ba/Al_2O_3 catalyst. Besides, potassium is another element that has shown potential as a storage component with a significant benefit at higher temperatures as the K-based nitrate is more stable than the typical Ba nitrate [14]. Therefore, it is believed that the new generation of LNT catalyst Pt/K/TiO_2–ZrO_2 is promising to be extensively used for lean-burn emission abatement. Takahashi et al. [15] have studied the influence of TiO_2 to ZrO_2 ratio on NO_x storage and sulfur-resistance performance of the LNT catalyst. It is shown that the optimal Ti/Zr atomic ratio is 4:6. However, after calcination at a high temperature of 800 °C [12], it is found that TiO_2–ZrO_2 binary oxides show low specific surface areas. Imagawa et al. [16, 17] found that the thermal aggregation of TiO_2–ZrO_2 particles can be inhibited in the presence of Al_2O_3 particles. They also indicated that the LNT catalyst using the ternary oxides synthesized by co-precipitation as a support shows larger NO_x storage capacity than that using the physical mixture of Al_2O_3 and TiO_2–ZrO_2 binary oxides as a support. Even so, the effect of Al_2O_3 doping on the storage routes and sulfur-resistance performance of TiO_2–ZrO_2 supported catalysts has not been investigated systematically, and the Al content in the support is never optimized, either. Therefore, this work focuses on the investigation of the NO_x storage mechanism and sulfur-resistance performance of Al_2O_3–TiO_2–ZrO_2 supported LNT catalysts, and the optimization of Al content. The catalysts using TiO_2–ZrO_2 and pure Al_2O_3 as supports were also prepared and investigated for comparison. The NO_x adsorption and storage, and sulfur adsorption and desorption behaviors over these LNT catalysts were characterized by in situ diffuse reflectance infrared spectroscopy (DRIFTS) and temperature-programmed reduction by hydrogen (H_2-TPR).

2 Experimental

2.1 Catalyst Preparation

TiO_2–ZrO_2 binary oxide support with a molar ratio of 4:6 was prepared by co-precipitation in an aqueous solution containing titanium tetrachloride and zirconium oxychloride. Aqueous ammonia was used as the precipitation reagent. The precipitate was kept at room temperature for 24 h, then filtered and washed with deionized water until no chloride ions were detected by $AgNO_3$ solution. After drying at 120 °C for 24 h, the precipitate was calcined at 800 °C for 5 h in air to obtain the final support TiO_2–ZrO_2, denoted as TZ. The ternary oxide supports Al_2O_3–TiO_2–ZrO_2 with different Al/(Ti + Zr) ratios of 1/3, 1/1 and 3/1 were prepared in the similar way above, denoted as ATZ(1/3), ATZ(1/1) and ATZ(3/1), respectively. The Al source used here is $Al(NO_3)_3{\cdot}9H_2O$.

The catalysts were prepared by sequential impregnation. At first, the synthesized support was impregnated with an aqueous solution of $H_2PtCl_6{\cdot}6H_2O$, then dried at 120 °C overnight and calcined at 250 °C for 1 h in air to obtain the precursor, which was subsequently impregnated in an aqueous solution of CH_3COOK. After drying at 120 °C overnight and calcination at 750 °C for 2 h, the final powder sample was pressed, crushed and sieved to 40–60 mesh. The loadings of Pt and CH_3COOK are 1 and 7 wt%, respectively. Before experiments, the samples were reduced at 500 °C for 1 h in a gas of 10 vol% H_2 in N_2. The final catalysts are denoted as Pt/K/TZ, Pt/K/ATZ(1/3), Pt/K/ATZ(1/1) and Pt/K/ATZ(3/1), respectively. For comparison, the sample Pt/K/Al_2O_3 was also prepared by the same procedure above using commercial γ-Al_2O_3 precalcined at 800 °C as a support.

2.2 Catalyst Characterization

The measurement of the specific surface area (S_{BET}) was carried out at −196 °C on Quantachrome QuadraSorb SI instrument by using the nitrogen adsorption method. The samples were pretreated in vacuum at 300 °C for 4 h before experiments. The specific surface area (S_{BET}) was determined from the linear part of the BET curve.

XRD patterns were recorded on an X'pert Pro diffractometer (PANAlytical Company) with a rotating anode using Co Kα as radiation source ($\lambda = 0.1790$ nm) at 40 kV and 40 mA. The data of 2θ from 10° to 90° range were collected with the step size of 0.02°.

Temperature-programmed reduction (TPR) measurement was conducted on a TPDRO 1100 apparatus supplied by Thermo-Finnigan company. Before detection by the TCD, the gas was purified by a trap containing CaO + NaOH materials in order to remove the H_2O and CO_2. Each time, 30 mg of the sample was heated from room temperature to 900 °C at a rate of 10 °C/min. A mixture gas consisting of H_2 and N_2 with H_2 content of 5% (volume percentage) was used as reductant with a flow rate of 20 mL/min. The operation condition is close to the well-known TPR criteria of Monti and Baiker equation [18].

In situ diffuse reflectance infrared spectroscopy (DRIFTS) measurement was performed on a Nicolet Nexus spectrometer equipped with a MCT detector cooled by liquid nitrogen, and an in situ chamber allowing the sample heated up to 600 °C. The NO_x sorption experiments over different samples were carried out at 350 °C. The powder sample (15 mg) was firstly pretreated in He at 350 °C for 30 min to record the background spectrum. Then 400 ppm NO + 5% O_2 in N_2 was introduced to the sample cell, and the spectra were collected at different exposure time up to 60 min. The flow rate of the mixture gas was 50 mL/min.

For NO_x adsorption at different temperatures, the steps were the same as described above. The temperature was increased from 200 to 500 °C at 50 °C interval. The powder sample was firstly pretreated in He at every temperature for 15 min and then the background spectrum was recorded. After exposure to NO + O_2 for 30 min at each temperature, the DRIFT spectra were collected.

The DRIFTS spectra of SO_2 adsorption on different samples at 400 °C were also recorded and the steps were similar to those for NO adsorption except that the adsorptive gas was changed into the mixture of 200 ppm SO_2, 5 vol%O_2 and the balance N_2.

2.3 NO_x Storage Capacity (NSC) Measurement, Sulfur-Aging and Regeneration Treatment

NSC measurements were carried out in a quartz-tubular continuous flow reactor (i.d. = 8 mm) containing 1.2 g of each catalyst (40–60 mesh). After the temperature reached 350 °C, a gas mixture of 400 ppm NO, 5% O_2 and the balance N_2 was introduced at a rate of 400 mL/min, corresponding to a space velocity of 20,000 h^{-1}. The concentrations of NO, NO_2, and total NO_x at the reactor outlet were monitored by a Chemiluminescence NO–NO_2–NO_x Analyzer (Model 42*i*-HL, Thermo Scientific).

For sulfur-aging experiments, 400 mg catalyst was used, each exposed to a gas containing 200 ppm SO_2, 5% O_2 and the balance N_2 at 400 °C for 2 h, with a flow rate of 160 mL/min. The ratio of the molar ratio of the total amount of SO_2 flowing through the catalyst in the fixed-bed reactor to the amount of K in the aged catalyst is 0.55, which ensures that the deep sulfation can be achieved if all the K is transformed into K_2SO_4. The regeneration of sulfur-aged catalysts was performed in a gas containing 10 vol% H_2 in N_2 at 500 °C for 60 min using 400 mg of the sulfur-aged catalyst.

The NO_x storage capacities of the regenerated catalysts were also measured. The procedure was same to fresh catalysts but 400 mg of each regenerated catalyst was used, corresponding to a space velocity of 60,000 h^{-1}.

3 Results and Discussion

3.1 XRD and BET Results

XRD test was performed in order to investigate the bulk structure of all the samples. From the XRD patterns of the fresh samples shown in Fig. 1, it can be seen that $ZrTiO_4$ appears in all the samples except Pt/K/Al_2O_3. However, the corresponding peaks get weaker with the contents of Ti and Zr decreasing, implying the decreased crystallite size of $ZrTiO_4$. It is noted that the peak around $2\theta = 59.0°$ should be contributed not only by $ZrTiO_4$ but also by tetragonal ZrO_2. Though $ZrTiO_4$ phase (PCPDFWIN 74-1504) also shows a peak at $2\theta = 59.5°$, the intensity of which should be weaker than the peaks at $2\theta = 62.0°$ and 63.6° which are close to the peak at $2\theta = 59.5°$. However, the peak in Fig. 1 around $2\theta = 59.0°$ is stronger than the two peaks at higher angle positions close to itself. At the same time, tetragonal ZrO_2 phase (PCPDFWIN 79-1769) shows the first strongest peak at $2\theta = 35.2°$ and the second strongest peak at $2\theta = 59.0°$. Therefore, it is reasonable to assign the peak around $2\theta = 59.0°$ to the total diffraction effect of $ZrTiO_4$ and ZrO_2.The strongest peak of ZrO_2 may be covered by the peak at $2\theta = 35.5°$ corresponding to $ZrTiO_4$. This interpretation above is very consistent with the ratio of Ti to Zr in the samples of 4/6, that is to say, the molar percentage of Zr is larger than that of Ti. Most of the Zr oxides reacted with Ti oxides to form $ZrTiO_4$ during calcination at 800 °C and then excess Zr component were segregated in the form of ZrO_2.

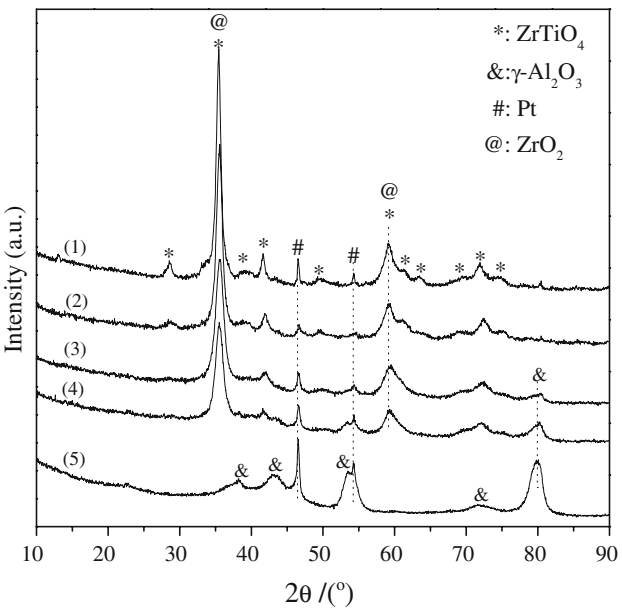

Fig. 1 XRD patterns of the fresh samples (*1*) Pt/K/TZ, (*2*) Pt/K/ATZ(1/3), (*3*) Pt/K/ATZ(1/1), (*4*) Pt/K/ATZ(3/1), (*5*) Pt/K/Al_2O_3

As shown in Fig. 1, γ-Al_2O_3 phase clearly appears on the sample Pt/K/Al_2O_3 with pure Al_2O_3 as a support. However, the peak at $2\theta = 80.0°$ corresponding to γ-Al_2O_3 also appears on the sample Pt/K/ATZ(3/1) and Pt/K/ATZ(1/1), indicating that the supports of the two samples are mixtures of $ZrTiO_4$, ZrO_2 and γ-Al_2O_3. Metallic Pt can be found on all the samples from Fig. 1 and the sample Pt/K/Al_2O_3 shows much stronger diffraction peaks of Pt compared to other samples, indicative of the largest Pt particles on Al_2O_3 support. The absence of the diffraction peaks of K phases suggests that K component is well dispersed on the supports or present in amorphous state.

The XRD patterns of sulfur-aged samples are shown in Fig. 2. All the sulfur-aged samples display the same diffraction patterns with the fresh samples except Pt/K/Al_2O_3. Two very small but visible peaks ascribed to K_2SO_4 can be found on the XRD pattern of sulfur-aged Pt/K/Al_2O_3. This means that SO_2 is easier to react with the K species supported on Al_2O_3, suggesting the inferior sulfur-resistance ability of the sample Pt/K/Al_2O_3 to other samples containing $ZrTiO_4$. After regeneration of the sulfur-aged samples, their XRD patterns are almost the same as those of the fresh samples (figure not shown). However, the very weak peak at 1,120 cm^{-1} assigned to K_2SO_4 can be found on the IR spectra of the regenerated samples (figure not shown). Theses results indicate that most of the sulfur species have been removed after regeneration and the residual amount of K_2SO_4 can hardly detected by XRD but only by IR.

The specific surface areas of the supports TiO_2–ZrO_2, TiO_2–ZrO_2–Al_2O_3 and pure Al_2O_3 as well as their corresponding catalysts are shown in Table 1. It is evident that

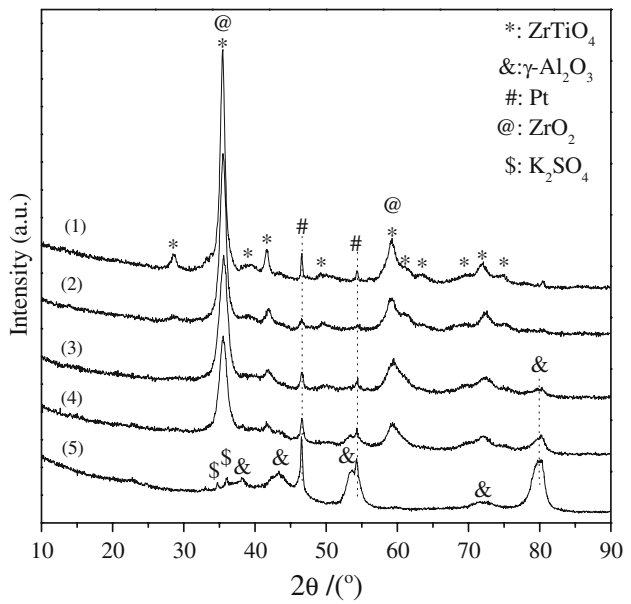

Fig. 2 XRD patterns of the sulfur-aged samples (*1*) Pt/K/TZ, (*2*) Pt/K/ATZ(1/3), (*3*) Pt/K/ATZ(1/1), (*4*) Pt/K/ATZ(3/1), (*5*) Pt/K/Al_2O_3

Table 1 Specific surface area of the supports and corresponding catalysts

Sample	Support (m^2/g)	Catalyst (m^2/g)
Pt/K/TZ	30	24
Pt/K/ATZ(1/3)	62	43
Pt/K/ATZ(1/1)	103	72
Pt/K/ATZ(3/1)	118	95
Pt/K/Al_2O_3	138	134

pure Al_2O_3 shows the largest surface area due to its good thermal stability while TiO_2–ZrO_2 possesses the lowest surface area of only 30 m^2/g. As expected, Al_2O_3 doping into the binary oxide TiO_2–ZrO_2 increased its surface area obviously, and with the content of Al increasing, the surface area of ternary oxide was further elevated. This result is consistent with the XRD result above where the crystallite size of $ZrTiO_4$ decreases with Al content increasing.

After the support was impregnated with Pt and *K*, the corresponding catalyst always shows a lower surface area than pure supports. For pure Al_2O_3 this decrease is not significant while for other supports a decrease in the range of 20–30% can be observed. Even so, the sequence among different catalysts is also the same as that among different supports, indicating that the Al content plays an important role in keeping high specific surface areas of the final catalysts.

3.2 In situ DRIFTS of NO and O_2 Co-adsorption

Although nano-composite Al_2O_3–TiO_2–ZrO_2 has ever been synthesized by Imagawa et al. [16], the NO_x storage routes of the LNT catalyst with K supported on this kind of ternary oxides support have not been investigated before. Recently we have reported the NO_x storage routes over Pt/K/TiO_2–ZrO_2 using the binary oxides TiO_2–ZrO_2 as a support [13]. To make clear of the NO_x storage routes over the K based LNT catalysts using Al_2O_3–TiO_2–ZrO_2 ternary oxides as supports, in situ DRIFTS experiment was carried out at different temperatures over all the samples. It is found that the spectra for all the five samples are almost the same, so the DRIFTS spectra of NO + O_2 co-adsorption on the sample Pt/K/ATZ(1/1) were selected as a representative to be shown in Fig. 3. It can be seen that the spectra are obviously temperature dependent. When the adsorption temperature is as low as 200 °C, a peak appears at 1,248 cm^{-1}, indicating the formation of plenty of free nitrite ions [14]. The appearance of another very weak peak at 1,376 cm^{-1} suggests the formation of a small quantity of free nitrate ions [14]. When the temperature is elevated to 250 °C, the peak at 1,248 cm^{-1} has disappeared while the peak associated with nitrates gets stronger. This means that the increased temperature favors the activation of oxygen species and then contributes the oxidation of nitrites to

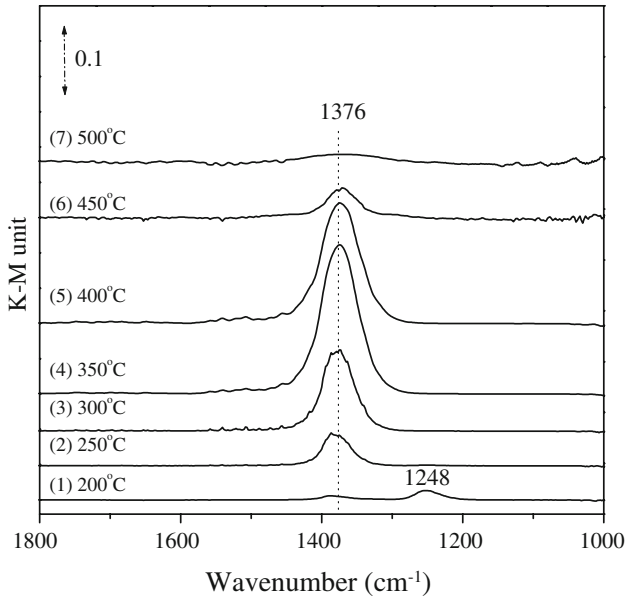

Fig. 3 In situ DRIFTS spectra of NO + O_2 adsorption over Pt/K/ATZ(1/1) at different temperatures for 30 min

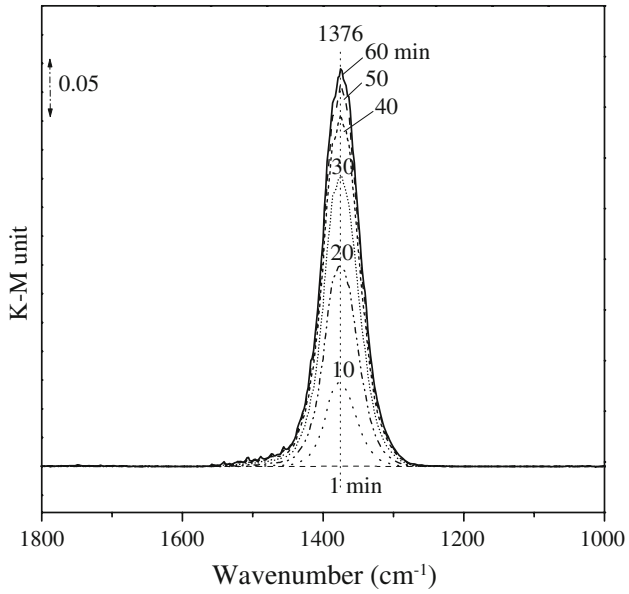

Fig. 4 In situ DRIFTS spectra of NO + O_2 adsorption over Pt/K/ATZ(1/1) at 350 °C for different time

nitrates. However, when the adsorption temperature is higher than 350 °C, the nitrate-related peak decreases gradually, since high temperature leads to the decomposition of nitrate. Up to 500 °C, the nitrate decomposes completely. In a summary, the NO_x storage routes depend strongly on the temperature. At a low temperature of 200 °C, NO_x storage should mainly proceeds via nitrite intermediates while at the temperature above 250 °C, NO_x storage mainly follows nitrate route. The optimal temperature for NO_x trapping efficiently as nitrate is around 350 °C, which is in line with the results obtained for Pt/K/TiO_2–ZrO_2 catalysts in previous study [13].

Figure 4 shows the DRIFTS spectra of NO + O_2 co-adsorption over Pt/K/ATZ(1/1) at 350 °C for different time. As expected, nitrate is the only intermediate, the peak intensity of which is increased with time going. However, after 30 min, the nitrate peak gets stronger more slowly than before, indicative of a slow NO_x storage process. There are two possible explanations for this. On the one hand, as proposed in previous study [13], the storage sites of K species on the catalyst surface can be divided into two categories: one adjacent to Pt, and another away from Pt, since the amount of K loading is much larger than that of Pt. The close contact of Pt sites with K sites can effectively promote the storage process by oxygen spillover from Pt sites to K sites, making the rapid NO_x storage as nitrate over these K sites. On the K sites away from Pt, NO_2 can not be immediately oxidized to nitrate, and nitrites could not be oxidized into nitrates timely, either, due to the lack of active oxygen from Pt sites. Therefore, the formation of nitrate on K sites away from Pt is slower than that on K sites adjacent to Pt. On the other hand, the storage process is also related to the dispersion of K species. Although no evident bulk K_2O or K_2CO_3 can be detected by XRD, it is still considered that K species exists in two states, namely the highly dispersed phase and relatively large crystallites phase which is still below XRD detection limit. The NO_x storage on highly dispersed potassium phase should be much quicker than on large crystallites potassium phase because of the surface to bulk diffusion limitation.

3.3 In situ DRIFTS of SO_2 Adsorption

Figure 5 shows in situ DRIFTS spectra of SO_2 + O_2 co-adsorption on the fresh LNT catalysts at 400 °C for 30 min. The band at 1,143 cm^{-1} related to sulfate [7, 12, 19, 20] can be clearly observed for the sample Pt/K/TZ. After doping Al_2O_3 into TiO_2–ZrO_2 support, this peak shifts to 1,200 cm^{-1} and it shifts to 1,215 cm^{-1} for the pure Al_2O_3 supported sample. However, the IR spectra of all the sulfur-aged samples used for XRD test (not shown here) exhibits a main peak at 1,120 cm^{-1}, which is consistent with that of the reference sample K_2SO_4 and the value reported in literature [21]. Furthermore, the evident bulk K_2SO_4 can be found from XRD on the sample Pt/K/Al_2O_3. On the one hand, this apparent inconsistency between IR results of sulfur-aged samples and DRIFTS results seems to be due to the differences in SO_2 treatment. For XRD and IR experiments, and aliquot of each catalyst was placed in a flow reactor and treated in diluted SO_2 flow at 400 °C for 2 h whereas for in situ DRIFTS experiments, the treatment was done in the DRIFTS in situ reactor in diluted SO_2 flow at 400 °C for 30 min. On the other hand,

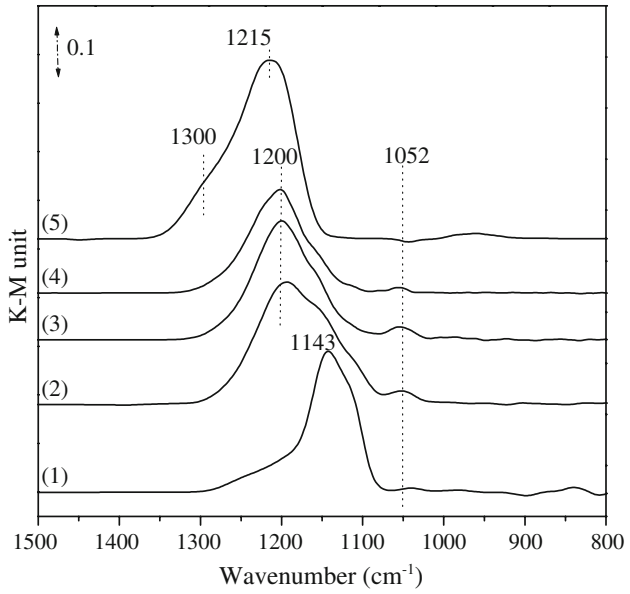

Fig. 5 In situ DRIFTS spectra of $SO_2 + O_2$ adsorption on the fresh samples at 400 °C (*1*) Pt/K/TZ, (*2*) Pt/K/ATZ(1/3), (*3*) Pt/K/ATZ(1/1), (*4*) Pt/K/ATZ(3/1), (*5*) Pt/K/Al_2O_3

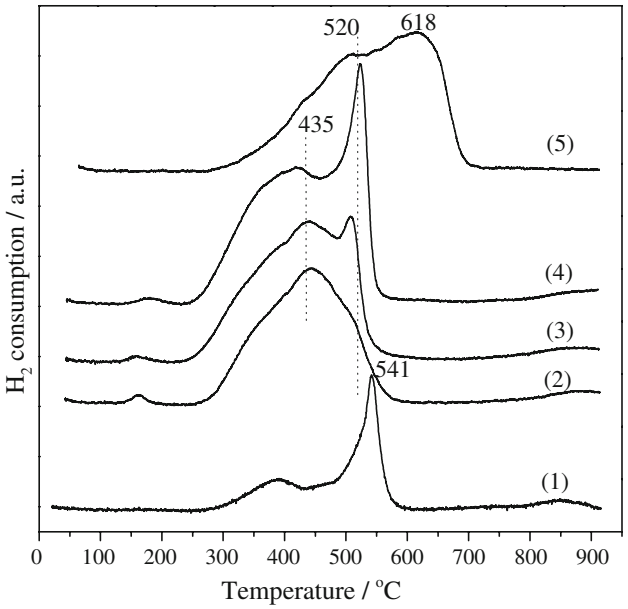

Fig. 6 H_2-TPR profiles of sulfur-aged samples (*1*) Pt/K/TZ, (*2*) Pt/K/ATZ(1/3), (*3*) Pt/K/ATZ(1/1), (*4*) Pt/K/ATZ(3/1), (*5*) Pt/K/Al_2O_3

the shifts of peak to higher wave numbers after Al_2O_3 doping may result from the different configuration of sulfate on the samples. It is reported that different configuration of SO_4^{2-} can form on the surface of metal oxides, such as unidentate, chelating bidentate and bridged bidentate [22, 23]. For SO_2 and O_2 co-adsorption on the sample Pt/K/TZ, the formation of unidentate sulfate associated with K_2O is possible. However, when Al_2O_3 was doped into TiO_2–ZrO_2, much bridged bidentate sulfate may have formed with the sulfur atom bonded to the surface oxygen of K_2O and Al_2O_3 simultaneously due to the basicity of Al_2O_3. Consequently, higher wave number can be observed for the Al_2O_3 containing samples in Fig. 5. The small shoulder band at 1,300 cm^{-1} for Pt/K/Al_2O_3 suggests the existence of a small quantity of surface $Al_2(SO_4)_3$ [20]. In Al_2O_3 doped samples, the existence of trace $Al_2(SO_4)_3$ is also potential, whose band may be covered by that of K_2SO_4. Besides these, the very small peak at 1,052 cm^{-1} for all the samples is also resulted from the vibration mode of sulfate group [19]. From the intensity of the main bands related to sulfate, it is inferred that more sulfur species have deposited on Al_2O_3 supported sample, indicative of its worse sulfur-resistance performance, the use of ternary oxides Al_2O_3–TiO_2–ZrO_2 as support decreased the sulfur deposition to some extent.

3.4 H_2-TPR Results

H_2-TPR experiments were performed on sulfur-aged catalysts to investigate the sulfur desorption behavior, and the results are presented in Fig. 6. For the Pt/K/TZ catalyst, the profile is very similar to that reported in our previous study [12] for Pt/K/TiO_2–ZrO_2, though the two catalysts were calcined at different temperatures and different Ti/Zr ratios were adopted during preparation. As previously interpreted, the peak at relatively low temperature of 390 °C can be attributed to the reduction of sulfate species formed from –OK groups, and that at relatively high temperature of 541 °C perhaps corresponds to the reduction of potassium sulfate derived from the highly dispersed K_2O. It is observed that a very wide desorption peak from 300 to 700 °C appears for the sample Pt/K/Al_2O_3, which should be related to the reduction of bulk sulfate, since K_2SO_4 has been found over this sample from XRD results. Besides, it cannot be ruled out that the reduction of surface $Al_2(SO_4)_3$ is included in this extremely wide reduction peak. By comparison, it is obvious that the sulfur desorption from the sulfur-aged catalyst Pt/K/Al_2O_3 is the most difficult, indicative of its worst regeneration ability. For the catalysts using ternary oxides Al_2O_3–TiO_2–ZrO_2 as supports, the main reduction peak of sulfate appears around 435 °C, much lower than those of Pt/K/Al_2O_3 and Pt/K/TZ, suggesting remarkably improved regeneration performance. Worth noting that a small peak at 520 °C emerges for the three samples and it gets stronger with Al content increasing. Therefore, this peak can be ascribed to the reduction of surface $Al_2(SO_4)_3$, which is in good agreement with the analysis of DRIFTS spectra of SO_2 adsorption that the existence of surface $Al_2(SO_4)_3$ is possible after sulfation. The extremely weak peak below 200 °C in Fig. 6 occurs on the three samples with ternary oxides as supports, which may be due to the reduction of some PtO*x*

species in the three sulfur-aged samples. From the XRD peaks of Pt on the fresh samples shown in Fig. 1, it can be inferred that the Pt particles in these three samples with ternary oxides as supports are smaller than those in the sample Pt/K/TZ and Pt/K/Al_2O_3. Therefore, during sulfation treatment, the smaller Pt particles may be easier reoxidized than the larger ones. However, the XRD patterns of the sulfur-aged samples shown in Fig. 2 suggest that metal Pt is always the main Pt species. So, only partial smaller Pt particles in the three samples were reoxidized during sulfation. As a whole, the catalysts with ternary oxides Al_2O_3–TiO_2–ZrO_2 as supports show much lower sulfur desorption temperatures compared to the catalysts with TiO_2–ZrO_2 or pure Al_2O_3 as a support, suggesting their much better sulfur-resistance performance. At the same time, the desorption temperature is also much lower than that for traditional Pt/Ba/Al_2O_3 LNT catalysts [6, 7].

3.5 NO_x Storage Behaviors

Isothermal experiments of NO_x storage were carried out over all the samples at 350 °C since the DRIFTS results of NO adsorption have revealed that the samples show the largest NO_x storage capacity at this temperature. Figure 7 shows the change of outlet concentrations of NO_x with time after the feed gas was switched to the fresh catalysts bed, and Fig. 8 shows those for the regenerated catalysts. The NO_x storage amounts, calculated by integrating the concentration curves, are listed in Table 2. From Fig. 7, it can be seen that before NO_x concentration reaches its rock bottom, the concentration decreases very quickly, implying a fast storage process. However, after this process, the NO_x concentration gets back to its inlet concentration at a lower and lower speed, indicating a slow storage process. The reason has been elucidated in detail in Sect. 3.2. From Table 2, it is found that the NSC for all the fresh catalysts is much lower than the theoretic NSC (714 μmol/g) calculated from the K loading, assuming that all the K species can be utilized for NO_x storage. Besides, the NSC increases with Al content increasing and the catalyst with pure Al_2O_3 as support shows the largest NSC. This can be explained as follows from two sides. On the one hand, the transformation from K_2O or K_2CO_3 to nitrates is limited by thermodynamic equilibrium. On the other hand, the potassium species in Pt/K/TiO_2–ZrO_2 can react with TiO_2 via solid-phase-reaction, leading to the deactivation of some K species [15]. Therefore, it is reasonable that the experimental NSC is lower than the theoretic NSC. The elevation of the atomic ratio of Al/(Ti + Zr) is equal to lowering Ti content, making more potassium usable. Additionally, the increased specific surface area with Al content increasing should also increase the NO_x storage amount by better dispersing K species.

After sulfation at 400 °C and regeneration at 500 °C, the NSC of each catalyst has decreased seen from Fig. 8 and

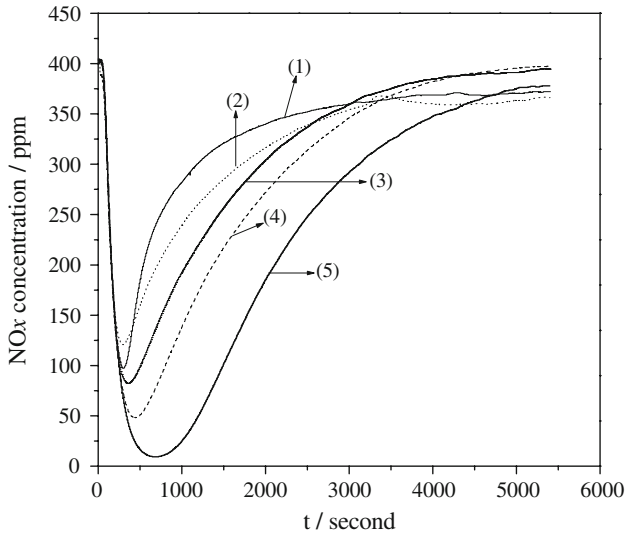

Fig. 7 Outlet concentration of NO_x versus time over the fresh samples (*1*) Pt/K/TZ, (*2*) Pt/K/ATZ(1/3), (*3*) Pt/K/ATZ(1/1), (*4*) Pt/K/ATZ(3/1), (*5*) Pt/K/Al_2O_3

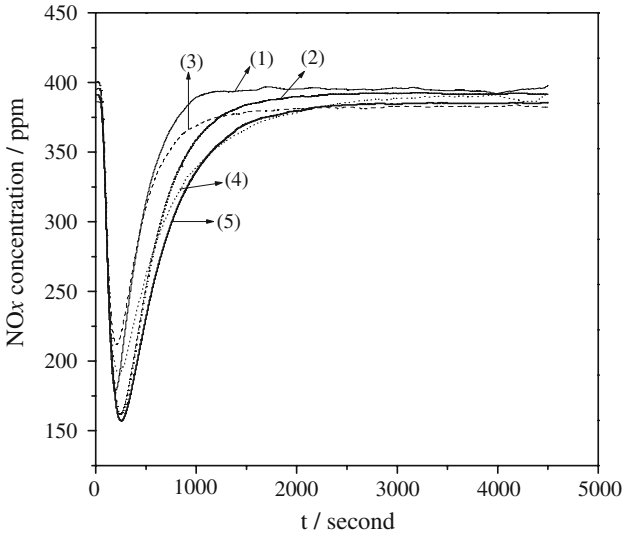

Fig. 8 Outlet concentration of NO_x versus time over the regenerated samples (*1*) Pt/K/TZ, (*2*) Pt/K/ATZ(1/1), (*3*) Pt/K/Al_2O_3, (*4*) Pt/K/ATZ(1/3), (*5*) Pt/K/ATZ(3/1)

Table 2 NO_x storage capacity (NSC) of the samples

Sample code	Fresh sample (μmol/g)	After regeneration (μmol/g)	Recovery efficiency(%)
Pt/K/TZ	96	60	62.5
Pt/K/ATZ(1/3)	116	105	90.5
Pt/K/ATZ(1/1)	125	120	96.0
Pt/K/ATZ(3/1)	158	128	81.0
Pt/K/Al_2O_3	227	69	30.4

Table 2. However, the regenerated catalysts with ternary oxides Al_2O_3–TiO_2–ZrO_2 as supports show obviously much larger NSC than that for those with binary oxide TiO_2–ZrO_2 or pure Al_2O_3 as a support. The recovery efficiency of Pt/K/TZ is only 62.5% while 81–96% of recovery efficiency can be achieved when Al_2O_3 was added into the TiO_2–ZrO_2 support. Besides, the recovery efficiency decreased to only 30.4% for the catalyst supported on pure Al_2O_3. This result indicates that the best sulfur-resistance can be obtained over the catalyst supported on Al-contained ternary oxides. The NSC of the regenerated catalyst and its recovery efficiency should be closely related to the desulfation behavior of the catalysts. As seen in Fig. 6, the sulfate desorption is the most difficult over the sample Pt/K/Al_2O_3, so, the recovery of K storage sites in this sample is least efficient, showing a low NSC (69 μmol/g) after sulfation and regeneration. In contrast, the lower sulfur desorption temperature can be found for the catalysts with ternary oxides as the supports, and therefore, both high NSC and recovery efficiency can be retained. In literature, it is ever suggested that the acidity of $ZrTiO_4$ can prevent SO_2 adsorption and promote SO_2 desorption, and Pt/K/TiO_2–ZrO_2 catalyst is promising due to its good sulfur-resistance [12, 15]. In this study, it is found that the doping of proper amount of Al_2O_3 into TiO_2–ZrO_2 binary oxides can further not only increase its NO_x storage capacity but also improve its sulfur-resistance performance by increasing the thermal-resistance of the support and promoting the sulfur desorption from the sulfur-aged catalyst. Among the ternary oxides supported catalysts investigated here, the catalyst with the atomic ratio of Al/(Ti + Zr) of 3/1 always shows the highest NSC before or after sulfation-regeneration, which is promising for the practical use in lean-burn NO_x abatement.

4 Conclusions

The doping of Al_2O_3 into TiO_2–ZrO_2 oxides can improve both the NSC and sulfur-resistance performance of the LNT catalyst Pt/K/TiO_2–ZrO_2. Therefore, the *K*-based LNT catalyst with ternary oxides Al_2O_3–TiO_2–ZrO_2 as a support is more promising for application in lean-burn NO_x abatement. NO_x storage on this catalyst mainly proceeds via nitrite intermediate at the temperature lower than 200 °C, while at the temperature above 250 °C, NO_x storage mainly follows nitrate route. The optimal temperature for NO_x trapping as nitrates is around 350 °C. Compared with the *K*-based LNT catalysts with TiO_2–ZrO_2 or pure Al_2O_3 as supports, the catalysts with Al-containing ternary oxides as the supports show much better sulfur-resistance performance due to the much easier desorption of sulfur. After sulfation-regeneration, the catalysts supported on the ternary oxides possess much larger NSC. At the same time, the high NSC recovery efficiency of 81–96% can be achieved over the catalysts supported on ternary oxides Al_2O_3–TiO_2–ZrO_2 while only 30.4 and 62.5% were obtained over the catalysts supported on pure Al_2O_3 and TiO_2–ZrO_2 oxides, respectively. The optimal atomic ratio of Al/(Ti + Zr) is 3/1 from the view of both the NO_x storage capacity and the sulfur-resistance performance.

Acknowledgments This work is financially supported by the National Natural Science Foundation of China (No. 20876110), the Program of New Century Excellent Talents in University of China (NCET-07-0599). The authors are also grateful to the "863" Programs of the Ministry of Science and Technology of China (2008AA06Z323), the Natural Science Foundation of Tianjin (No. 07JCYBJC15100) and the Cheung Kong Scholar Program for Innovative Teams of the Ministry of Education (No. IRT0641).

References

1. Shinjoh H, Takahashi N, Yokota K, Sugiura M (1998) Appl Catal B 15:189
2. Matsumoto S (2004) Catal Today 90:183
3. Courson C, Khalfi A, Mahzoul H, Hodjati S, Moral N, Kiennemann A, Gilot P (2002) Catal Commun 3:471
4. Engström P, Amberntsson A, Skoglundh M, Fridell E, Smedler G (1999) Appl Catal B 22:L241
5. Takeuchi M, Matsumoto S (2004) Top Catal 28:151
6. Matsumoto S, Ideka Y, Suzuki H, Ogai M, Miyoshi N (2000) Appl Catal B 25:115
7. Sedlmair C, Seshan K, Jentys A, Lercher JA (2002) Catal Today 75:413
8. Amberntsson A, Skoglundh M, Jonsson M, Fridell E (2002) Catal Today 73:279
9. Amberntsson A, Skoglundh M, Ljungström S, Fridell E (2003) J Catal 217:253
10. Yamazaki K, Suzuki T, Takahashi N, Yokota K, Sugiura M (2001) Appl Catal B 30:459
11. Luo JY, Meng M, Zha YQ, Xie YN, Hu TD, Zhang J, Liu T (2008) Appl Catal B 78:38
12. Liu Y, Meng M, Li XG, Guo LH, Zha YQ (2008) Chem Eng Res Des 86:932
13. Liu Y, Meng M, Zou ZQ, Li XG, Zha YQ (2008) Catal Commun 10:173
14. Toops TJ, Smith DB, Partridge WP (2006) Catal. Today 114:112
15. Takahashi N, Suda A, Hachisuka I, Sugiura M, Sobukawa H, Shinjoh H (2007) Appl Catal B 72:187
16. Imagawa H, Tanaka T, Takahashi N, Matsunaga S, Suda A, Shinjoh H (2007) J Catal 251:315
17. H. Imagawa, T. Tanaka, N. Takahashi, S. Matsunaga, A. Suda, H. Shinjoh, Appl. Catal. B (2008), doi:10.1016/j.apcatb.2008.07.019
18. Monti DAM, Baiker A (1983) J Catal 83:323
19. Fanson PT, Horton MR, Delgass WN, Lauterbach J (2003) Appl Catal B 46:393
20. Abdulhamid H, Fridell E, Dawody J, Skoglundh M (2006) J Catal 241:200
21. Peralta MA, Milt VG, Cornaglia LM, Querini CA (2006) J Catal 242:118
22. Chen JP, Yang RT (1993) J Catal 139:277
23. Lavalley JC (1996) Catal Today 27:377